Journal of Wind Engineering & Industrial Aerodynamics 218 (2021) 104767

Contents lists available at ScienceDirect

Journal of Wind Engineering & Industrial Aerodynamics

journal homepage: www.elsevier.com/locate/jweia

Narrowband components in two-celled tornado-like vortices generated in a Ward-type simulator

Delong Zuo [a,*], Zhuo Tang [a], Hui Zhang [a], Darryl James [a], Yuzuru Eguchi [b]

[a] National Wind Institute, Texas Tech University, 1009, Canton Ave, Lubbock, TX, USA
[b] Civil Engineering Research Laboratory, Central Research Institute of Electric Power Industry, Abiko, 1646, Abiko-shi, Chiba-ken, Japan

ARTICLE INFO

Keywords:
Tornado-like vortex
Turbulence
Surface pressure
Narrowband components

ABSTRACT

While many studies have been conducted to characterize tornado-like flows, most of the knowledge resulting from these studies is on the mean components of the flows. This paper presents a study aimed at further understanding the turbulence in tornado-like vortices simulated in a Ward-type simulator as well as the fluctuations of the pressures on the surface beneath the simulated vortices. The focus is placed on the narrowband components that have been discovered in both the flows of two-celled vortices and the surface pressures caused by these vortices. The dependences of the characteristic frequency of the narrowband components and the spatial distributions of the standard deviations of these components in the flow and pressure fields on the swirl ratio and radial Reynolds number of the vortices are investigated. The relationship between some observed characteristics of the flow and the corresponding characteristics of the surface pressure are also interpreted to investigate the mechanism that produces the narrowband components.

1. Introduction

As a type of violet windstorm, tornadoes continue to leave behind long trails of destructions that cause excessive life and property losses. According to the Storm Events Database of the National Oceanic and Atmospheric Administration (NOAA) (https://www.ncdc.noaa.gov/stormevents/textsearchhelp.jsp), tornadoes are responsible for more than 900 fatalities and $22B of direct property damages in the past decade in the United States alone. In addition, losses and damages such as these have caused interruptions to social and economic functions that often take communities significant time to recover from.

The persistent devastations have motivated numerous studies of tornadoes as an atmospheric phenomenon as well as the impact of tornadoes on the built environment. Many studies, in particular, have been performed based on laboratory experiments in tornado simulators, which were conceptualized by Ying and Chang (1970) and have since evolved into a number of different types, including the classical Ward type (Ward, 1972) and the type that follows the design of the simulator at Iowa State University (Haan et al., 2008). Early experiments in tornado simulators (e.g., Church et al., 1979; Ward, 1972) were primarily used to study the characteristics of tornado-like vortices and their dependence on the swirl ratio, the radial Reynolds number and the aspect ratio, which are the parameters that control the dynamics and geometry of the vortices (Davies-Jones, 1973; Lewellen, 1962). Among the many findings from these experiments, it was particularly revealed that tornado-like flow transitions from a single-celled vortex to a two-celled vortex and finally to multiple sub-vortices as the swirl ratio increases. In addition to directly characterizing the velocities of the flows in tornado-like vortices, some early experiments in tornado simulators were also used to investigate the pressures on the surface beneath the flows (subsequently referred to as surface pressures) (e.g., Pauley et al., 1982; Snow et al., 1980). These experiments suggested that the transition of the flow with increasing swirl ratio is accompanied by corresponding transition of the surface pressure characteristics, such as the shape of the radial profile of the mean surface pressure deficit.

In the past two decades, a number of modern tornado simulators were built and used to further investigate the characteristics of tornado-like flows and the pressure deficits caused by the flows (e.g., Haan et al., 2008; Refan and Hangan, 2016; Tang et al., 2018a; Wang et al., 2017). In addition, many experiments were also conducted in these simulators to study tornado-like loading on buildings and other structures. For example, Haan et al. (2010) and Feng and Chen (2018) studied the

* Corresponding author.
E-mail addresses: delong.zuo@ttu.edu (D. Zuo), Zhuo.tang@ttu.edu (Z. Tang), hui.zhang@ttu.edu (H. Zhang), darryl.james@ttu.edu (D. James), eguchi@criepi.denken.or.jp (Y. Eguchi).

https://doi.org/10.1016/j.jweia.2021.104767
Received 6 November 2020; Received in revised form 11 August 2021; Accepted 4 September 2021

loading on a gable-roofed low-rise building model by tornado-like vortices and the dependence of the loading on the speed at which the vortices translate; Razavi and Sarkar (2018) investigated the effects of some major factors, including the swirl ratio and translation speed of the vortex and the configuration of a low-rise building model in terms of the orientation and position of the model relative to the mean path of the translating vortex, on the tornado-like loading; Sabareesh et al. (2012) quantified the influence of the roughness of the surrounding surface on the tornado-like loading of a low-rise building model. While these studies mainly focused on the pressure on the external surface of the building envelope, a number of other studies (e.g., Letchford et al., 2015; Rajasekharan et al., 2013; Roueche et al., 2020; Thampi et al., 2011) were also used to characterize the internal pressure of low-rise buildings exposed to tornado-like vortices. In addition to revealing many characteristics of tornado-like loading on models of low-rise buildings, a number of these studies also compared tornado-like loading with loading by boundary-layer-type winds (e.g., Feng and Chen, 2018; Haan et al., 2010; Roueche et al., 2020), resulting in the discovery that the difference between these two types of loading can be very significant.

Although previous experimental studies in tornado simulators have significantly advanced the understanding of tornado-like flows and their loading on structures, most studies of the flows focused on the mean components of the velocities and the mean pressure deficits caused by the flows, and the interpretation of tornado-like loading often used the mean characteristics of the velocities and pressure deficits as references. Only a limited number of studies have comprehensively investigated the turbulence in tornado-like vortices generated in tornado simulators or the fluctuation of the surface pressure. For example, Tari et al. (2010) investigated the characteristics of the normal and shear stresses of tornado-like flows of various swirl ratios; Refan et al. (2015) examined the variation of turbulence intensity with swirl ratio for tornado-like flows generated both in a large simulator and in a scaled-down model of this large simulator; Tang et al. (2018a) and Tang et al. (2018b) quantified the first four moments of the velocities over portions of single-celled and two-celled vortices generated at two aspect ratios as well as the first four moments of the surface pressures caused by these vortices, and Karami et al. (2019) used the techniques of proper orthogonal decomposition and dynamic proper orthogonal decomposition to investigate the prominent mechanisms of tornado-like vortices of various swirl ratios and identify coherent dynamic components in the flow. In addition, Eguchi et al. (2018) numerically reproduced the near-floor pressure fluctuation measured in a tornado simulator with consideration of the effects of turbulence.

This paper presents a further study of the turbulence in tornado-like flows generated in a tornado simulator and the fluctuations of the surface pressures caused by the flows. The focus is placed on the narrowband components that have been observed for the first time both in the turbulence of the flow in two-celled vortices and in the surface pressures caused by these vortices. The dependence of the characteristic frequency and the spatial distributions of the narrowband components on the swirl ratio and the radial Reynolds number are evaluated. Based on the observations, the potential mechanism that produces the narrowband components in the flow are also investigated. In addition to further advancing the understanding of the turbulence in tornado-like flows, the outcomes of this investigation can also contribute to future studies of tornadic loading on structures.

2. Experimental facility

The tornado-like vortices subjected to study were generated in the large-scale Ward-type simulator (Ward, 1972), VorTECH, at Texas Tech University. This simulator, which has been used previously to characterize stationary tornado-like vortices of various swirl ratios, aspect ratios and radial Reynolds numbers (Tang et al., 2018a, 2018b), has been upgraded recently to accommodate studies of loading on structures by translating tornado-like vortices. As schematically shown in Fig. 1, the simulator has a testing chamber of 10.2 m in diameter and an updraft hole of $r_0 = 2$ m in radius. The updraft is provided by 8 fans at the top, and a honeycomb is used to decouple the rotation of the updraft from the axial component. After the upgrade, the height (h) of the chamber as well as those of the 64 turning vanes installed around the periphery of the chamber to guide the directions of the inflow can be varied between 0.7 m and 1.7 m. The center section of the upgraded simulator floor is mounted on an aluminum truss system and separated from the rest of the floor. Electric motors can drive this center section to move on steel rails at velocities up to 1.47 m/s (over 5.5 m at this maximum speed). This enables models of structures to translate through vortices generated by the simulator.

3. Experimental configurations

As has been established by the early pioneering studies (e.g., Church et al., 1979; Davies-Jones, 1973; Lewellen, 1962), the characteristics of tornado-like flows are controlled by the swirl ratio, the radial Reynolds number and the aspect ratio. In this study, these controlling parameters are defined as

$$S = r_0\Gamma / (2Qh) \tag{1}$$

$$Re_r = Q / (2\pi\nu) \tag{2}$$

$$a = h/r_0 \tag{3}$$

where$S$, Re_r and a are the swirl ratio, the radial Reynolds number and the aspect ratio, respectively, ν is the kinematic viscosity of air, and Q and Γ are the volume flow rate per unit axial length and the circulation, respectively. While the determination of h and r_0 is straightforward, especially for a Ward-type simulator, the manner in which Q and Γ were estimated in previous studies have varied. In this study, Q and Γ are estimated based on measurements of flow velocities at points along a vertical line originating from the edge of the updraft hole, following the scheme used by Tang et al. (2018a):

$$Q = 2\pi r_0 \sum_{n=1}^{N} \left(\overline{V}_{r,n} \times \Delta h_n \right) \Big/ h \tag{4}$$

$$\Gamma = 2\pi r_0 \times \sum_{n=1}^{N} \left(\overline{V}_{\theta,n} \times \Delta h_n \right) \Big/ h \tag{5}$$

where $\overline{V}_{r,n}$ and $\overline{V}_{\theta,n}$ are the mean velocities of the radial and tangential components of the flow, measured by a Cobra probe (Turbulent Flow Instrumentation Pty Ltd), at the nth point along the vertical line, Δh_n is half the distance between the two measurement points surrounding this point, and N is the total number of measurement points along the vertical line.

It is noted that alternative definitions for the swirl ratio have been used in studies of tornado-like vortices. For example, an often used alternative definition of the swirl ratio is $S = \tan\theta/(2a)$, in which θ is the angle of the turning vanes relative to the relevant radial lines of the testing chamber (subsequently referred to as the vane angle). Refan and Hangan (2016) and Razavi and Sarkar (2018) compared this definition for the swirl ratio with the definition represented by equation (1). However, in the comparisons, the circulation, Γ in equation (1), was taken as that at the point where the mean tangential velocity is the maximum.

In the experiments, the floor of the simulator was kept stationary, and the height of the testing chamber as well as those of the turning vanes were fixed at 1 m, resulting in an aspect ratio of 0.5. To generate vortices of various swirl ratios and radial Reynolds numbers, the vane angle and the speeds of the fans were varied. Table 1 summarizes the swirl ratios and radial Reynolds numbers of the vortices and the

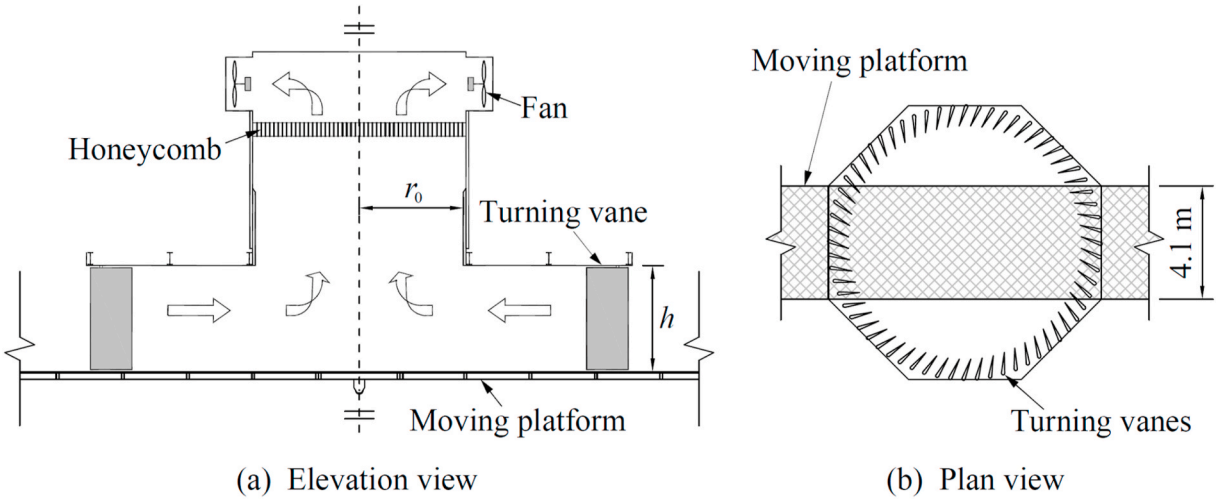

Fig. 1. (a) Elevation and (b) plan views of VorTECH.

Table 1
Configurations of vane angles and fan speeds and the corresponding swirl ratios and radial Reynolds numbers of the tornado-like vortices.

Config.	Vane Angle (°)	Fan speed (%)	S	Re_r ($\times 10^5$)	Velocity Measurement
1	6	100	0.17	6.46	Yes
2	8	100	0.21	6.38	
3	10	100	0.25	6.24	
4	14	100	0.35	6.05	
5	25	100	0.65	5.79	Yes
6	30	50	0.83	2.90	
7	30	60	0.83	3.48	Yes
8	30	70	0.83	4.07	
9	30	80	0.83	4.65	
10	30	90	0.83	5.19	
11	30	100	0.83	5.72	Yes

corresponding vane angles and fan speeds. The vane angles provided in this table enables a calculation of alternative swirl ratios according to $S = \tan\theta/(2a)$ if so desired.

As will be shown subsequently, the vortex with a swirl ratio of 0.17 is single-celled in structure; the vortices with swirl ratios of 0.35, 0.65 and 0.83 are two-celled in structure, and those with the other two swirl ratios (0.21 and 0.25) are close to the critical transition of the flow from a single-celled structure to a two-celled structure. The generation of these vortices enabled an evaluation of the differences in the characteristics of single-celled and two-celled vortices as well as those of the vortices close to the transition through either direct interpretation of flow velocity measurements or inferences based on measurements of surface pressures. In addition, the vortices with swirl ratios of 0.35, 0.65 and 0.83 were generated so that characteristics of two-celled vortices with swirl ratios ranging from smaller to larger values can be compared. The two vortices with different swirl ratios of 0.65 and 0.83 but nearly identical radial Reynolds number of 5.79×10^5 and 5.72×10^5 were generated to enable a study of the effects of swirl ratio on the characteristics of two-celled vortices. Similarly, the vortices with essentially the same swirl ratio of 0.83 but various radial Reynolds numbers were used to reveal the effects of radial Reynolds number on the characteristics of these vortices. The particular radial Reynolds numbers are chosen so that the effects of radial Reynolds number over a broad range can be assessed. Because the radial Reynolds numbers of full-scale tornadoes are many magnitudes larger than those of the vortices that the simulator can generate, vortices with radial Reynolds numbers that are smaller than the smallest values shown in Table 1 were not considered.

For each vortex, a Scanivalve system was used to measure the surface pressures at 289 points along a radial line over a range of ±190 cm from the nominal center of the floor. As indicated in Table 1, measurements of flow velocities were also conducted for four of the vortices (indicated with the letter "Y"). The velocity measurements were taken by a Cobra probe and an Omniprobe (Aeroprobe Corporation) at a large number of points in a plane through the vertical axis of the vortex. The measurement started from the inlet side of the simulator using the Cobra probe and progressed in the radial direction towards the nominal axis of the vortex. At each point, the Cobra probe was first oriented with its tip aligned with the tangential direction of the flow. The measurement with this probe orientation was retained if 100% of the data are valid (i.e., the flow being within a ±45° cone originating from the tip of the probe) according to the manufacture-supplied software. Otherwise, the probe was rotated to provide measurements with various percentages of valid data. The best measurement was retained if at least 98% of the data recorded at that particular probe orientation are valid. When none of the measurements taken at the various probe orientations contains at least 98% of valid data, the Omniprobe was used to measure the velocity at that point as well as the points at the same height and further towards the vertical axis of the vortex. In this case, the Omniprobe was oriented with its head facing the approaching tangential component of the flow. Each measurement by the Omniprobe contains at least 93% of valid data according to the software supplied by the manufacturer. This is considered acceptable because these measurements are only used to characterize the mean and low-frequency components of the flows. As an illustration, Fig. 2 shows the velocity measurement grid for the vortex with a swirl ratio of 0.65 and a radial Reynolds number of 5.79×10^5. The resolutions of the grid in both the radial (r) and vertical (z) directions were varied to capture the rapid spatial variation of the flow in the region near the floor and around the radius of the vortex core. The vertical resolution of the velocity measurement was the same for all four vortices marked with "Y" in Table 1, but the measurement range and resolution in the radial direction were changed from vortex to vortex according to the variation of the flow characteristics along this direction. All the pressure and velocity measurements were conducted at a sampling frequency of 625 Hz. For each experimental configuration, the pressure measurements were repeated 10 times for 2-min durations, but the velocity measurements were performed only once for 2-min durations. Accordingly, every statistic of the pressure measurements to be presented subsequently is the average of the ten corresponding statistics estimated based on an ensemble of ten 2-min measurements. By contrast, the statistics of the velocity measurements are based on single 2-min measurements.

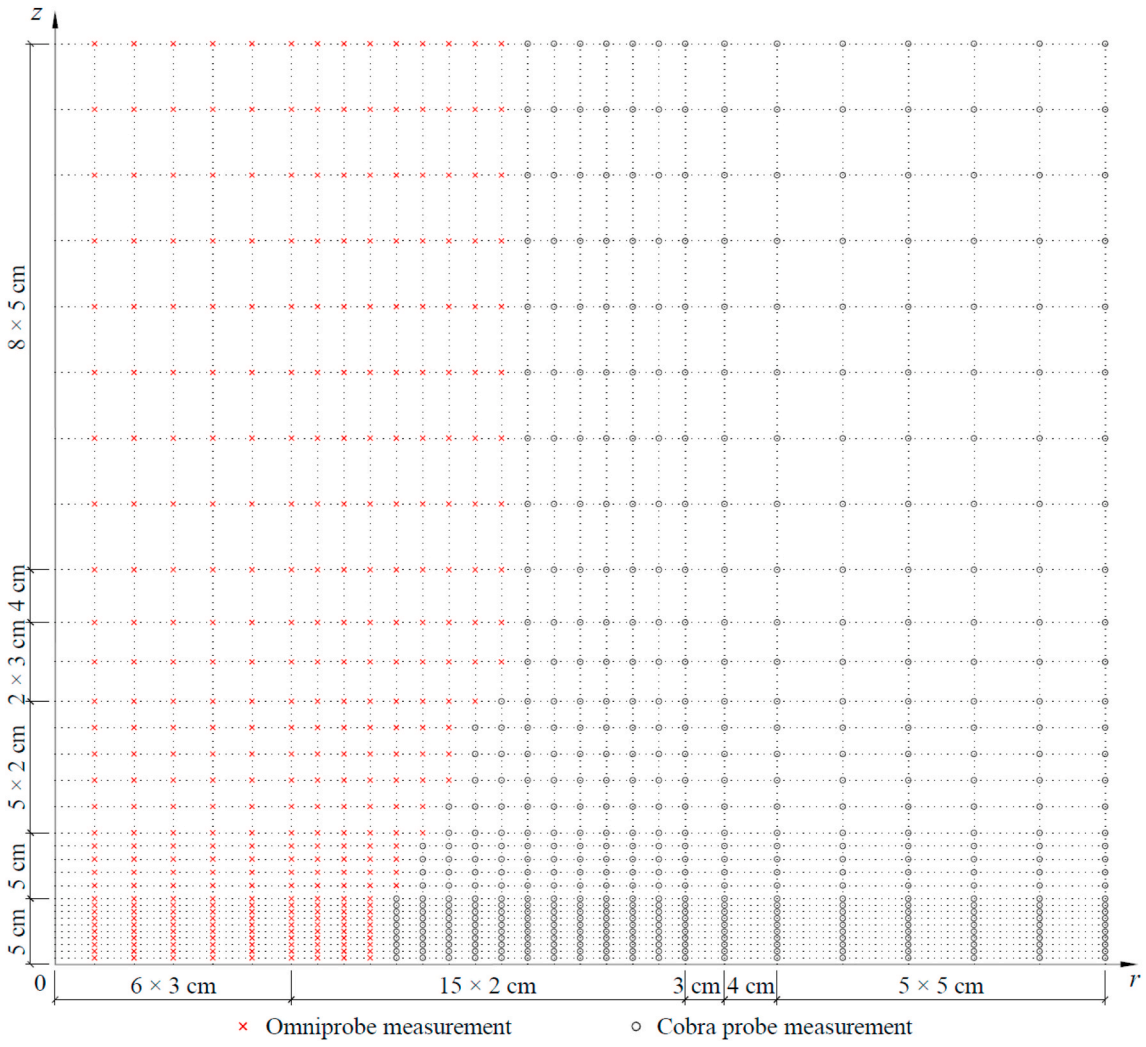

Fig. 2. Velocity measurement grid for the vortex with a swirl ratio of S = 0.65 and a radial Reynolds number of $Re_r = 5.79 \times 10^5$.

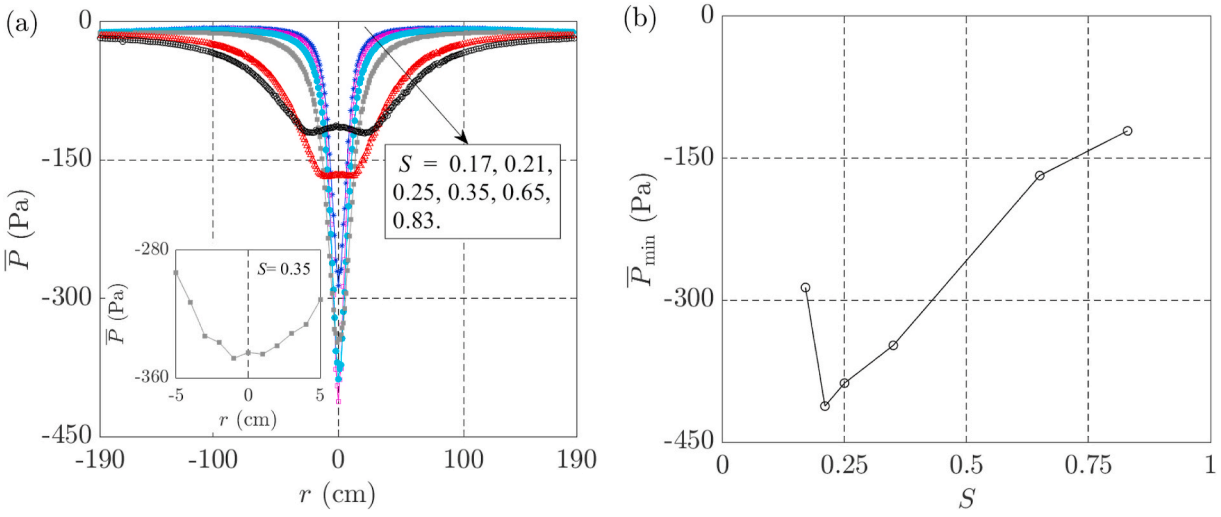

Fig. 3. (a) Radial profiles of the mean surface-pressures caused by vortices with various swirl ratios and, and (b) maximum mean surface-pressure deficit as a function of the swirl ratio.

4. Characteristics of narrowband components in surface pressures caused by two-celled vortices

As reported in many previous studies (e.g., Refan and Hangan, 2016; Snow et al., 1980; Tang et al., 2018a), the characteristics of tornado-like flows are reflected in the corresponding characteristics of surface pressures. For this reason, and because surface pressure measurement was conducted for every vortex generated in the experiments, the characteristics of the surface pressures are presented herein first.

Fig. 3 (a) shows the radial profiles of the mean surface pressure deficits (relative to the barometric pressure in a static bottle underneath the simulator floor), $\overline{P}$, caused by the tornado-like vortices generated with the fans at full speed, and Fig. 3 (b) shows the mean surface pressure deficit of the maximum magnitude ($\overline{P}_{\min}$) at each swirl ratio. Here r is the radial position measured from the nominal center of the simulator floor. According to previous studies (e.g., Tang et al., 2018a), as a vortex transitions from a single-celled structure to a two-celled structure with increasing swirl ratio, the radial profile of the mean surface pressure deficit transitions from a single-valleyed shape to a shape with two valleys, and the critical transition occurs when the maximum magnitude of the mean surface pressure deficit in the radial profile reaches the maximum value. Fig. 3 suggests, then, that the vortex with a swirl ratio of 0.17 is single-celled in structure, that those with swirl ratios of 0.35, 0.65 and 0.83 are two-celled in structure, and that the critical transition occurs at a swirl ratio close to 0.21. In addition, this figure also indicates that the change of flow characteristics after the transition is gradual, as the two-valleyed shape of the mean pressure deficit profile is much less well defined for the vortex with a small swirl ratio of 0.35 than for the two vortices with swirl ratios of 0.65 and 0.83. Also, because the vortices with swirl ratios of 0.21 and 0.25 are close to the critical transition, the radial profiles of the mean surface pressures caused by these vortices do not have two valleys.

The transition of the vortex from a single-celled structure to a two-celled structure with increasing swirl ratio is also reflected in the changes in the characteristics of the surface pressure fluctuation. For example, Fig. 4 shows the normalized (by $\left|\overline{P}_{\min}\right|$) radial profiles of the standard deviations, σ_p, of the surface pressures caused by the vortices generated with the fans at full speed. It can be seen that the profile associated with the single-celled vortex with a swirl ratio of 0.17 has a single peak. By contrast, the profiles associated with the two-celled vortices with swirl ratios of 0.35, 0.65 and 0.83 are bi-modal in shape. The profiles corresponding to the vortices with swirl ratios of 0.21 and 0.25 are similar in shape to that corresponding to the single-celled vortex with a swirl ratio of 0.17 because the flows in these two vortices are near the critical transition. These observations regarding the change of the radial profile of the standard deviations of the surface pressures due to the critical transition further confirms the identification of the vortex type based on the radial profile of the measure surface pressure.

The pressure measurements from the current study also confirms observations from previous studies (e.g., Tang et al., 2018a) that many major mean and fluctuating characteristics of the surface pressures are independent of the radial Reynolds number if the radial Reynolds number is sufficiently large. For example, Fig. 5 shows the radial profiles of the unnormalized and normalized (by $\left|\overline{P}_{\min}\right|$ for each case) mean values of the surface pressures caused by the vortices with the same swirl ratio of $S = 0.83$ but various radial Reynolds numbers. At each location, the mean surface pressure deficits caused by the vortices are apparently different. However, the profiles of the normalized mean surface pressure deficits collapse for the broad range of radial Reynolds numbers. Fig. 6 further shows the radial profiles of the normalized (by $\left|\overline{P}_{\min}\right|$) standard deviations of the surface pressures for the same vortices with the swirl ratio of $S = 0.83$ but various radial Reynolds numbers. It is evident that both the shape and magnitude of the normalized profiles are essentially independent of the radial Reynolds number.

A further examination of the pressure measurements reveals that the surface pressure fluctuations caused by the two-celled vortices contain distinct narrowband components. Fig. 7 show the contour plots of the power spectral density functions estimated based on the surface pressures measured beneath two of the two-celled vortices. Narrowband components with a characteristic frequency of 1.34 Hz can be clearly observed in the surface pressures caused by the vortex with a swirl ratio of $S = 0.65$ and a radial Reynolds number of $Re_r = 5.79 \times 10^5$. Similarly, it can be seen that the surface pressures caused by the vortex with a swirl ratio of $S = 0.83$ and a radial Reynolds number of $Re_r = 5.72 \times 10^5$ contain narrowband components with a characteristic frequency of 2.73 Hz. In addition, Fig. 7 suggests that for both cases, the narrowband components of the highest intensities occur at radial locations that are close to but not in the immediate vicinity of the center of the simulator

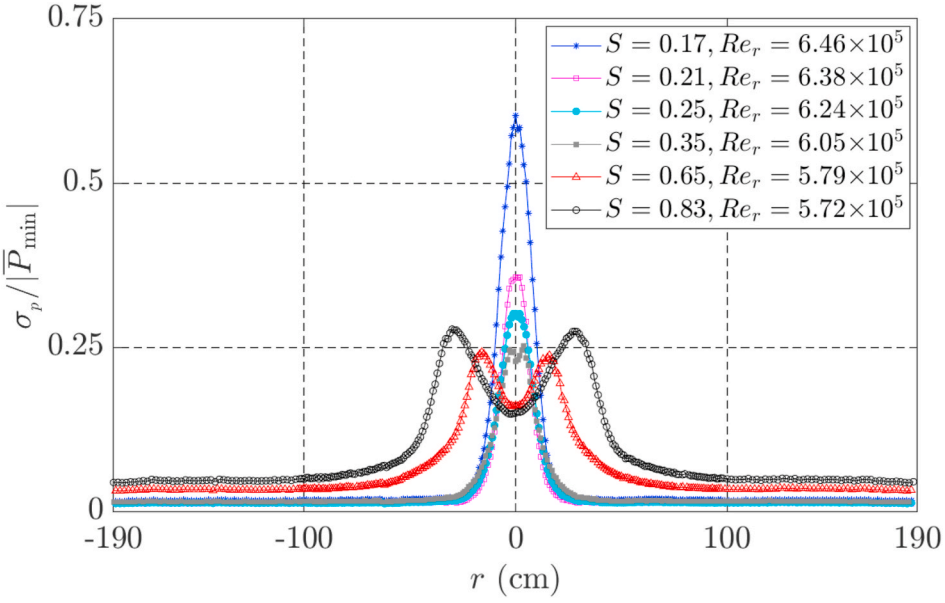

Fig. 4. Radial profiles of the standard deviations of the surface-pressures caused by vortices of various swirl ratios.

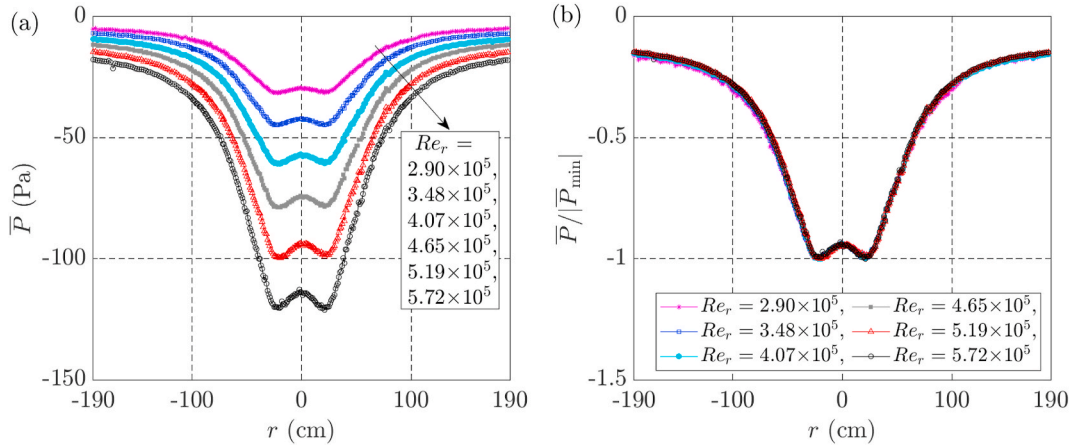

Fig. 5. Radial profiles of the (a) unnormalized and (b) normalized mean surface pressures caused by vortices with a swirl ratio of $S = 0.83$ and various radial Reynolds numbers.

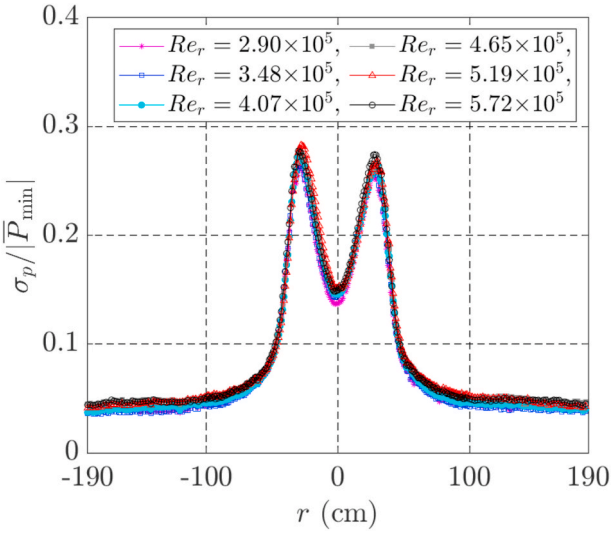

Fig. 6. Radial profiles of the normalized standard deviations of the surface pressures caused by vortices with a swirl ratio of $S = 0.83$ and various radial Reynolds numbers.

floor.

While the narrowband components in the surface pressures beneath the two-celled vortices with swirl ratios of $S = 0.65$ and $S = 0.83$ are strong compared with the components of other frequencies, the surface pressures caused by the two-celled vortex with a smaller swirl ratio of $S = 0.35$ are found to contain only weak narrowband components. Fig. 8 (a) depicts a contour plot of the estimated power spectral density functions of the surface pressures caused by the two-celled vortex with a swirl ratio of $S = 0.35$. Weak narrowband components with a characteristic frequency of 1.68 Hz can be observed in this figure at radial positions that are considerably far from the center of the simulator floor, and no clear signs of narrowband components are present at locations close to the center of the floor. The latter, however, is suspected to be because the narrowband components are weak and do not stand out against the other frequency components at these locations. When the flow continues to approach the critical transition between single-celled and two-celled structures as the swirl ratio decreases even f*f*$_c$urther, narrowband components disappear from the surface pressures. As an illustration, Fig. 8 (b) shows a contour plot of the estimated power spectral density functions of the surface pressures caused by the vortex with a swirl ratio of $S = 0.25$. No signs of narrowband components can be identified in this graph.

Fig. 7 clearly suggests that the characteristic frequency of the narrowband components in the surface pressures depends on the swirl ratio, as the narrowband components of different characteristic frequencies are caused by two vortices with different swirl ratios of $S =$

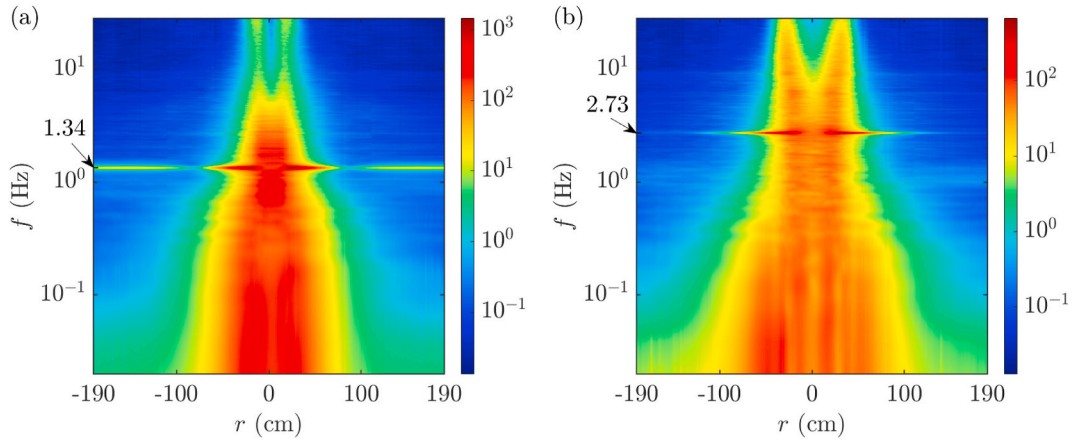

Fig. 7. Power spectral density functions (in Pa^2/Hz) of the surface pressures along a radial line beneath the two-celled vortices with (a) $S = 0.65$ and $Re_r = 5.79 \times 10^5$, and (b) $S = 0.83$ and.$Re_r = 5.72 \times 10^5$

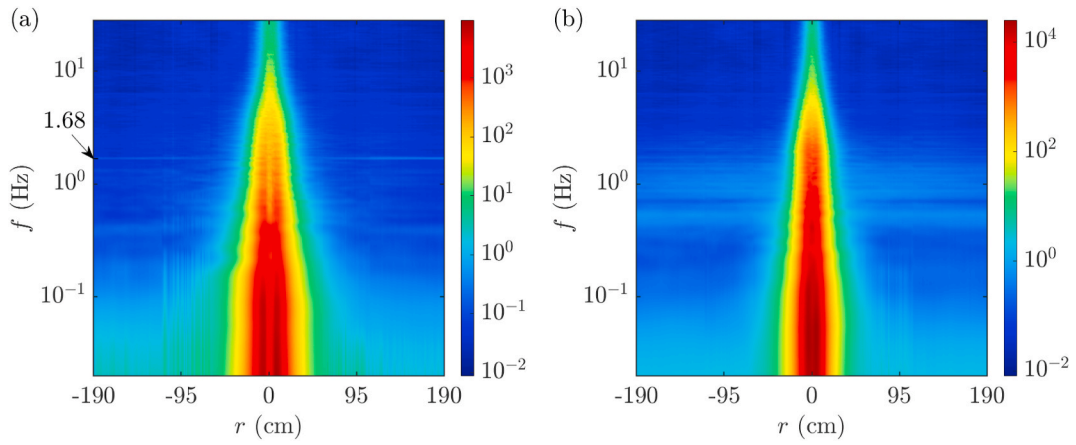

Fig. 8. Power spectral density functions (in Pa^2/Hz) of the surface pressures along a radial line beneath the two-celled vortices with (a) $S = 0.35$ and $Re_r = 6.05 \times 10^5$, and (b) $S = 0.25$ and.$Re_r = 6.24 \times 10^5$

0.65 and $S = 0.83$ but nearly identical radial Reynold numbers of $Re_r = 5.79 \times 10^5$ and $Re_r = 5.72 \times 10^5$. The surface pressure measurements also suggest that the characteristic frequency of the narrowband components has a definitive relationship with the radial Reynolds number. This can be seen in Fig. 9, which depicts the characteristic frequency of the narrowband components in the surface pressures, against the radial Reynolds number for the two-celled vortices with the same swirl ratio of $S = 0.83$ but different radial Reynold numbers. It is evident that the characteristic frequency increases approximately linearly with increasing radial Reynolds number. Since the radial Reynold number is proportional to the volume flow rate per unit axial length, which is proportional to the mean radial velocity of the inflow, this means that the characteristic frequency also increases linearly with increasing mean radial velocity of the inflow.

To extract the narrowband components in the surface pressures caused by two-celled vortices and enable an evaluation of the magnitudes and spatial distribution of these components, the measurements at each tap on the simulator floor are bandpass filtered using a 6th order Butterworth filter with a passing band of 0.2 Hz centered at the characteristic frequencies. Fig. 10 shows the radial profiles of the normalized

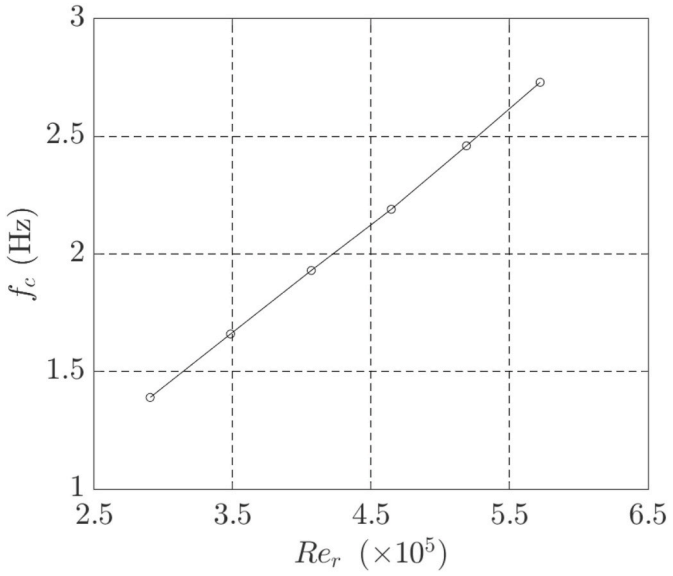

Fig. 9. Relationship between the characteristic frequency of the narrowband components in the surface pressures and the radial Reynolds number for two-celled vortices with a swirl ratio of.$S = 0.83$

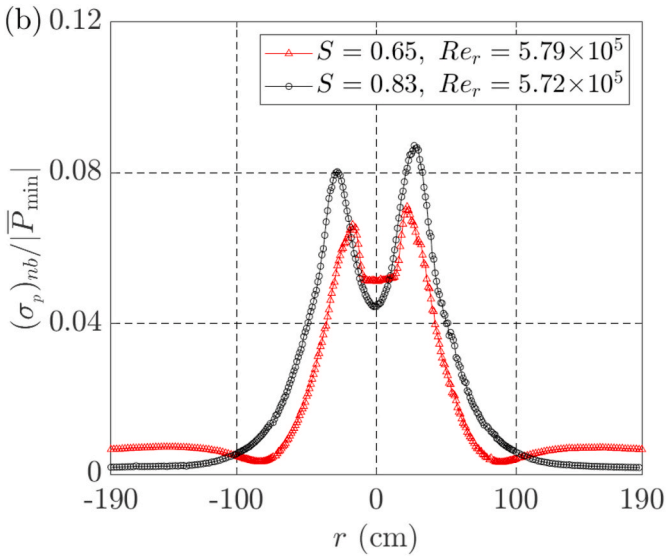

Fig. 10. Radial profile of the normalized standard deviations of the narrowband components in the surface pressures caused by two two-celled vortices.

(by $|\overline{P}_{\min}|$) standard deviations, $(\sigma_p)_{nb}$, of the narrowband components in the surface pressures caused by the two-celled vortices for which the power spectral density functions of the surface pressures are presented in Fig. 7. It is seen that for each vortex, the standard deviations of the narrowband components are the largest over regions that are close to but not in the immediate vicinity of the nominal center of the floor. This is consistent with what has been observed in Fig. 7. Fig. 10 also suggests that the radial profiles of the standard deviations of the narrowband components are bi-modal in shape, much like the shapes of the radial profiles of the standard deviation of the total surface pressures under these two vortices (Fig. 4). Although the bi-modal profiles appear to be asymmetric about the nominal center of the floor, this is primarily due to the imperfection of the experiments. Fig. 10 also shows that not only the magnitudes, but also the overall shapes of the two normalized radial profiles are different. Since the two vortices in question are of different swirl ratios but almost identical radial Reynolds numbers, this suggests that both the magnitudes and spatial distribution of the standard deviations of the narrowband components vary with the swirl ratio.

Fig. 11 presents the radial profiles of the normalized (by $|\overline{P}_{\min}|$) standard deviations of the narrowband components in the surface

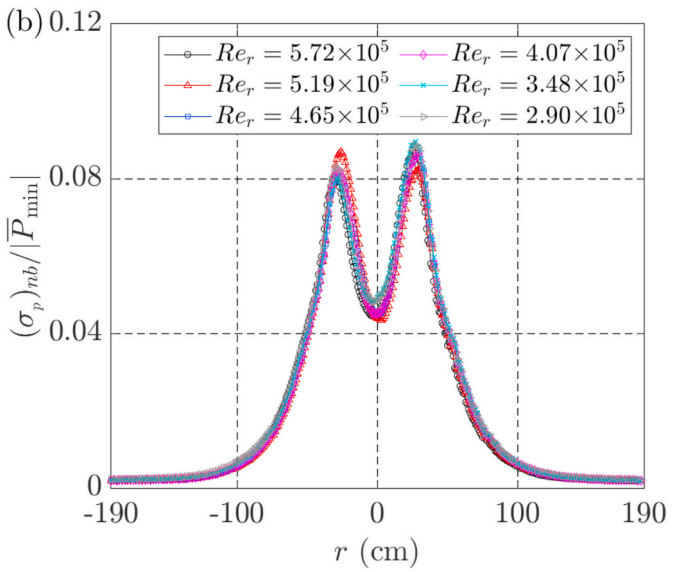

Fig. 11. Radial Profiles of the normalized standard deviations of the narrowband components in the surface pressures caused by two-celled vortices with a swirl ratio of $S = 0.83$ and various radial Reynolds numbers.

pressures caused by the two-celled vortices with the same swirl ratio of $S = 0.83$ but various radial Reynolds numbers. It is remarkable that all the normalized profiles essentially collapse for the broad range of radial Reynolds numbers despite the fact that the maximum mean pressure deficits ($\left|\overline{P}_{\min}\right|$) corresponding to these radial Reynold numbers are very different (Fig. 5). This suggests that although the characteristic frequency of the narrow-band component depends on the radial Reynolds number, as shown in Fig. 9, the relative magnitudes (i.e., normalized by $\left|\overline{P}_{\min}\right|$) of the narrowband components are essentially independent of the radial Reynolds number over the range considered.

5. Characteristics of narrowband components in the turbulence in the flow

The measurements show that the characteristics of the surface pressures, in particular those of the narrowband components, are indeed reflections of the corresponding characteristics of the flows aloft. The following presentation will focus primarily on the characteristics of the flows in the two-celled vortices, as narrowband components are identified only in these vortices.

Fig. 12 (a) and (b) show the mean velocity fields of the two-celled vortices with swirl ratios of $S = 0.65$ and $S = 0.83$, respectively, and redial Reynolds number of $Re_r = 5.79 \times 10^5$ and $Re_r = 5.72 \times 10^5$, respectively, over the vertical plane in which the velocity measurements were taken. The arrows in the graphs represent the resultants of the mean velocities of the radial and vertical components of the flow at the points of measurement, and the color represents the magnitude of the mean velocity of the tangential component ($\overline{V}_\theta$). Also in the graphs, z is the height above the simulator floor, and r_c, which will subsequently be referred to as the core radius of the vortex of interest, and z_c are the radial position and height above the simulator floor, respectively, at which the mean tangential velocity reaches the maximum magnitude. According to the mean velocity fields, the maximum mean tangential velocities in the two vortices both occur at heights close to the simulator floor. However, for the two vortices of almost the same radial Reynolds number, the core radius of the one with the larger swirl ratio of $S = 0.83$ ($r_c = 46$ cm) is much larger than that of the one with the smaller swirl ratio of $S = 0.65$ ($r_c = 26$ cm).

Furthermore, Fig. 12 suggests that both vortices consist of downdrafts in regions surrounding the vertical axis of the vortices. This confirms again the observation based on the radial profiles of the mean values and standard deviations of the surface pressures (Figs. 3 and 4) that these two vortices are two-celled in structure. With the assumption that the flow is axisymmetric and the fact that the flow swirls around the axis of the vortex, it can be observed from Fig. 12 (a) that the downdrafts in the vortex with the smaller swirl ratio of $S = 0.65$ are parts of a three dimensional, torus-like circulation around the vertical axis of the vortex. This is evidenced by the mean structure of the flow in the approximate region circled in Fig. 12 (a). Specifically, it can be deduced that the downdrafts turn outward at heights close to the floor and follow that with subsequential upward, inward and downward turns to complete the vertical circulation while also moving in the tangential direction,

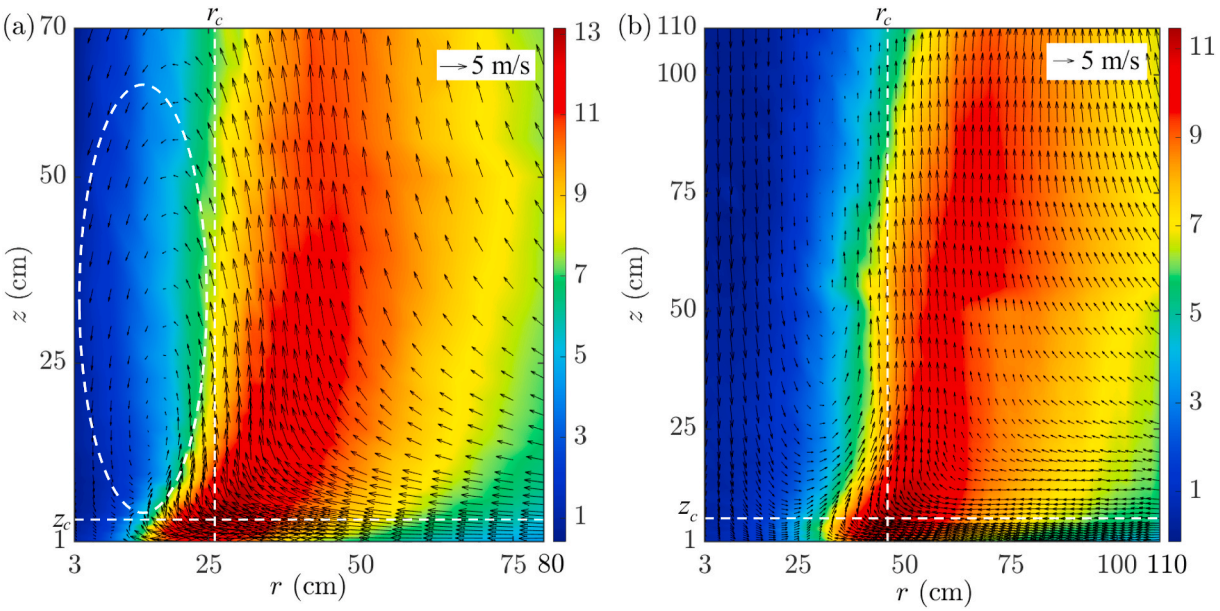

Fig. 12. Mean velocity (in m/s) fields of vortices with (a) $S = 0.65$ and $Re_r = 5.79 \times 10^5$, and (b) $S = 0.83$ and.$Re_r = 5.72 \times 10^5$

although this three-dimensional flow pattern cannot be directly visualized in the graph. A similar three-dimensional, torus-like circulation can be inferred in the mean velocity field of the vortex with the larger swirl ratio of $S = 0.83$ (see Fig. 12 (b)). However, a definitive observation cannot be made because the upper parts of the circulating flow in this vortex were not captured due to the difficulty in measuring flow velocities at heights beyond 110 cm above the simulator floor.

The velocity measurements also recorded narrowband components in the flows in the two-celled vortices that are counterparts of the narrowband components in the surface pressures caused by the flows. As an illustration, Fig. 13 shows the power spectral density functions, $S_{uu}(f)$, of the turbulence in the mean wind directions at the points where the mean tangential velocity in three of the two-celled vortices reaches the maximum magnitude. All the measurements based on which the power spectral density functions are estimated were carried out using the Cobra probe, so the turbulence can be considered to have been measured with adequate accuracy. This figure suggests that the flow at the location of interest in each vortex contains a narrowband component. In addition, this figure along with Figs. 7 and 9 suggests that for each vortex, the characteristic frequency of the narrowband component in the flow is the same as that of the narrowband components in the surface pressures. This is expected because the fluctuation of the surface pressure is a result of the turbulence in the flow aloft. Furthermore, this also suggests that the characteristic frequency of the narrowband component in the flow depends on the swirl ratio and radial Reynolds number in the same manner as does the characteristic frequency of the narrowband components in the surface pressures.

To enable an assessment of the spatial distribution of the narrowband components in the flows in the two-celled vortices, the turbulence components at every point of measurement in each two-celled vortex are bandpass filtered using a 6th order Butterworth filter with a pass band of 0.2 Hz centered at the characteristic frequency, and the turbulence kinetic energies of the resultant narrowband components are computed. Fig. 14 depicts the turbulence kinetic energies of the narrowband components in the two-celled vortices with swirl ratios of $S = 0.65$ and $S = 0.83$, respectively, and nearly identical radial Reynold numbers of $Re_r = 5.79 \times 10^5$ and $Re_r = 5.72 \times 10^5$, respectively. The measurements by both the Cobra probe and the Omniprobe are included because the narrowband components are of relatively low frequencies and can be measured by both probes with adequate accuracy. It is seen that for the

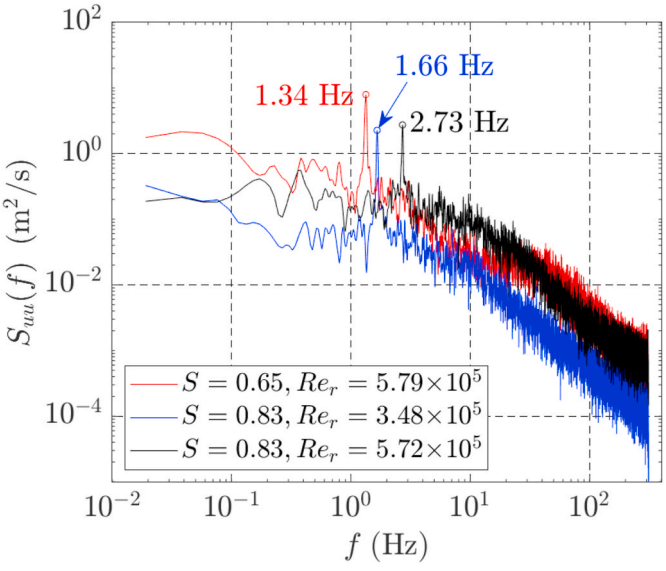

Fig. 13. Power spectral density functions of the turbulence in the mean wind direction at the location of the maximum mean tangential velocity in three two-celled vortices.

two vortices, the narrowband components of the highest intensities occur over different regions that span restricted ranges of radial and vertical locations. Since the two vortices are of different swirl ratios but nearly identical radial Reynold numbers, this suggests that the spatial distribution of the narrowband component in the flow depends on the swirl ratio. In particular, it is evident that the narrowband component of the highest intensities occur at levels close to the simulator floor for the vortex with the smaller swirl ratio of $S = 0.65$, but at much higher levels above the simulator floor for the vortex with the larger swirl ratio of $S = 0.83$. This appears to be related to a fact shown in Fig. 12 that the torus-like circulation of the flow occurs at much higher levels for the vortex with the larger swirl ratio than for the vortex with the smaller swirl ratio.

Although the swirl ratio affects both the characteristic frequency and spatial distribution of the narrowband component in the turbulence in a two-celled vortex, the radial Reynolds number, for the range considered, is found to affect the characteristic frequency (Fig. 9) and magnitude but not the spatial distribution of the narrowband component. Fig. 15 presents the spatial distributions of the normalized kinetic energy of the narrowband components, $\sqrt{(TKE)_{nb}}/\overline{U}$, in the two-celled vortices with the same swirl ratio of $S = 0.83$ but different radial Reynolds numbers of $Re_r = 3.48 \times 10^5$ and $Re_r = 5.72 \times 10^5$. Here $(TKE)_{nb}$ is the turbulence kinetic energy of the narrowband component, and $\overline{U}$ is the mean speed of the flow in the mean direction at the point of measurement. Although the radial Reynolds numbers are significantly different, the spatial distributions depicted in Fig. 15 (a) and (b) are very similar. In fact, the small differences between the spatial distributions can be primarily attributed to subtle differences in the experiments and the fact that the statistics shown are estimated based on only one 2-min measurement at each point, which inevitably results in uncertainties in the estimated statistics. Nonetheless, the similarity of the spatial distributions of the normalized turbulence kinetic energies of the narrowband components suggests that the spatial distribution of the narrowband component is independent of the radial Reynold number over the range considered. This corroborates the fact shown in Fig. 11 that the radial profiles of the normalized standard deviations of the narrowband components in the surface pressures collapse for vortices of the same swirl ratio but various radial Reynolds numbers.

Although the exact mechanism that produces the narrowband components in two-celled vortices remain to be definitively identified, the measurements show strong evidence that it is closely related to the characteristics of the flow in the corner flow region (e.g., Lewellen et al., 2000). For example, Figs. 12 and 14 suggest that for the near-floor flow in the two two-celled vortices in question, the narrowband component of the highest intensity occurs over the region where the outward flow originating from the downdraft at the center of the vortex converges with the inflow. This observation is corroborated by the spatial distribution of the narrowband components in the surface pressures caused by these vortices. As an illustration, Fig. 16 shows parts of the radial profiles of the normalized (by $\left|\overline{P}_{\min}\right|$) standard deviation of the narrow band components, $(\sigma_p)_{nb}$, as well as that of the components excluding the narrowband components, $(\sigma_p)_r$, in the surface pressures caused by the same two-celled vortices in question. By comparing this figure with Fig. 14, it is evident that for each vortex, both the narrowband components and the components excluding the narrowband components in the surfacer pressures as well as the turbulence kinetic energies of the narrowband components in the near-floor flow all reach the highest intensities over similar radial locations. This strongly indicates that the narrowband component in the flow in two-celled vortices originates from the high-intensity turbulence caused by the convergence of the inward and outward near-floor flows in the corner flow region. In particular, it is believed that the narrowband component embedded in the turbulence in a two-celled vortex is due to the instability of the shear layer caused by the convergence of the outward and inward flows, as the

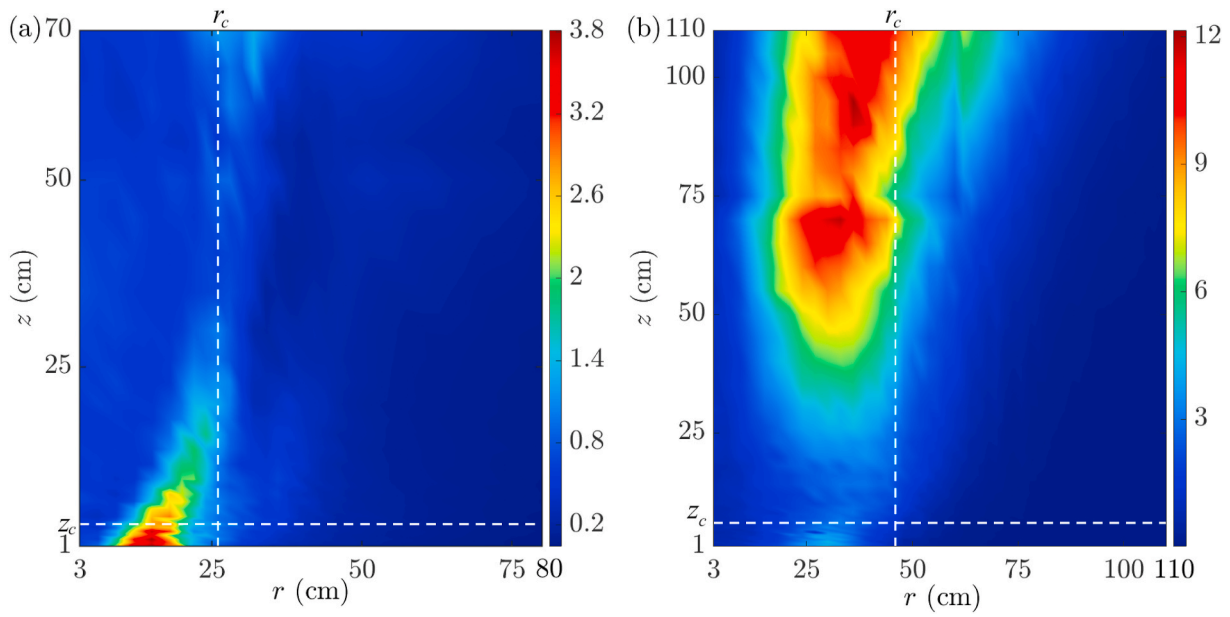

Fig. 14. Spatial distribution of the turbulence kinetic energies of the narrowband components (in m^2/s^2) in the vortices with (a) $S = 0.65$ and $Re_r = 5.79 \times 10^5$, and (b) $S = 0.83$ and.$Re_r = 5.72 \times 10^5$

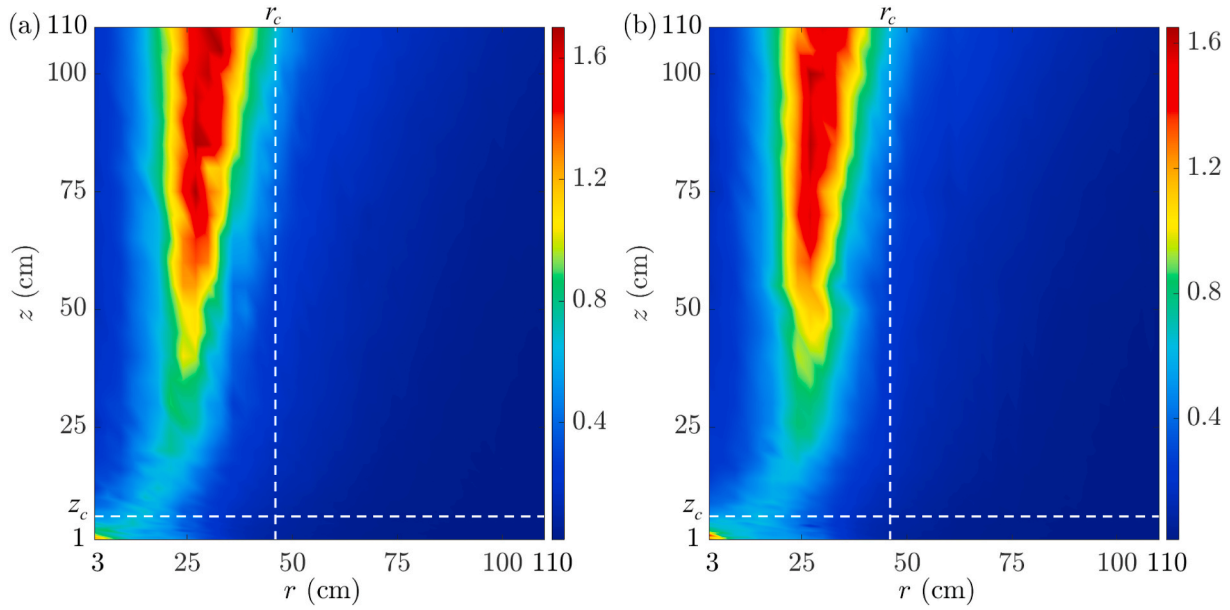

Fig. 15. Spatial distributions of the normalized turbulence kinetic energies of the narrowband components in two-celled vortices with the same swirl ratio of$S = 0.83$ and different radial Reynolds numbers of (a) $Re_r = 3.48 \times 10^5$ and (b) $Re_r = 5.72 \times 10^5$.

convergence of favorable and unfavorable pressure gradients in the near-wall region results in separation that likely contributes to the turbulence. The reason why the narrowband component in a specific vortex is of the specific characteristic frequency and spatial distribution observed, however, remains to be determined with further studies.

The evidence and its implications presented above also indirectly explains the reason why no narrowband component is observed in either the turbulence in the single-celled vortex generated in the experiments or the surface pressure fluctuations caused by the single-celled vortex. Fig. 17 depicts the mean velocity field of the single-celled vortex with a swirl ratio. It is apparent that this vortex does not contain downdrafts around its vertical axis that reach the simulator floor. As a result, there is not an outward flow component in the near-floor region to converge with the inward flow. Instead, the near-floor inward flow confluences in regions surrounding the vertical axis of the vortex and turns upward, as shown in Fig. 17, without producing a narrowband component in the flow.

6. Conclusions

To facilitate an investigation of the turbulence in tornado-like flows, vortices of various swirl ratios and radial Reynolds numbers were generated in a large-scale Ward-type simulator. The velocities of the flow at locations over a plane through the vertical axes of the vortices and the pressures at a large number of points along a radial line on the simulator floor were both measured. The pressure measurements confirm the observation from previous studies that the transition of the flow from a single-celled vortex to a two-celled vortex results in changes

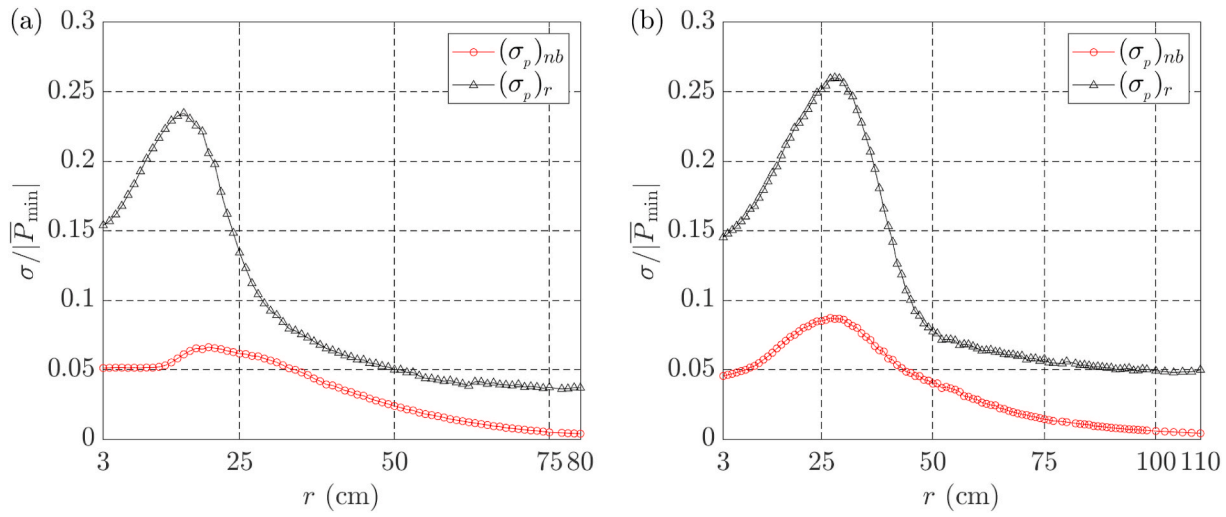

Fig. 16. Radial profiles of the normalized standard deviations of the components in the surface pressures caused by vortices of (a) $S = 0.65$ and $Re_r = 5.79 \times 10^5$, and (b) $S = 0.83$ and.$Re_r = 5.72 \times 10^5$

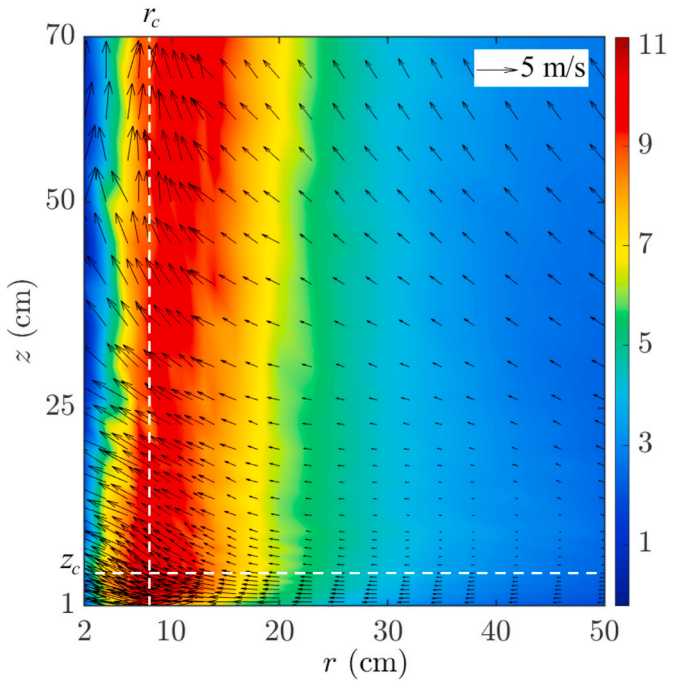

Fig. 17. Mean velocity (in m/s) field of a single-celled vortex with a swirl ratio of $S = 0.17$ and a Reynolds number of.$Re_r = 6.46 \times 10^5$

to the radial profiles of the mean values and standard deviations of the surface pressures. A further examination of the spectra of the pressure measurements also reveals the existence of narrowband components in the surface pressures caused by the two-celled vortices but not in the surface pressures caused by the single-celled vortex or the vortices near the transition from a single-celled structure to a two-celled structure. It is discovered that the characteristic frequency of the narrowband components in the surface pressures depends on both the swirl ratio and the radial Reynolds number of the two-celled vortex. In particular, for two-celled vortices of the same swirl ratio, the characteristic frequency of the narrowband components appears to depend linearly on the radial Reynolds number. In addition, while the magnitudes and spatial distribution of the narrowband components in the surface pressure are found to depend on the swirl ratio, only the magnitudes but not the spatial distribution of the narrowband components depend on the radial Reynolds number.

The characteristics of the surface pressures are found to be reflections of the corresponding characteristics of the flow aloft, as a narrowband component is also observed in the turbulence of the flow in each two-celled vortex, and the characteristic frequency of this narrowband component is found to be identical to the characteristic frequency of the narrowband components in the surface pressures caused by the flow. This suggests that the characteristic frequency of the narrowband component in the flow depends on the swirl ratio and the Reynolds number in the same manner in which the characteristic frequency of the narrowband components in the surface pressure depends on these two parameters. In addition, as in the case of the surface pressure fluctuations, it is observed that while both the magnitude and the spatial distribution of the narrowband component in the turbulence depend on the swirl ratio, the magnitude, but not the spatial distribution, of the narrowband component depends on the radial Reynolds number.

Lastly, narrowband component of the highest intensities in the near-floor flow as well as the narrowband components of the highest intensities in the surface pressures are both found to occur over the conner flow region over which the outward and inward near-floor flows in a two-celled vortex converge. It is believed based on this observation that the narrowband components in the flow are due to the instability in the shear layer that is caused by the convergence of the outward and inward flows.

CRediT authorship contribution statement

Delong Zuo: Supervision, Formal analysis, Participated in the internal review and revision of the paper, Funding acquisition. **Zhuo Tang:** Participated in experiment execution and the internal review and revision of the manuscript. **Hui Zhang:** Participated in the execution of the experiments. **Darryl James:** Supervision, Participated in the internal review and revision of the paper, Funding acquisition. **Yuzuru Eguchi:** Formal analysis, participated in the internal review and revision of the paper.

Declaration of competing interest

The authors declare that they have no known competing financial interests or personal relationships that could have appeared to influence the work reported in this paper.

Acknowledgement

This study is supported by the National Science Foundation under award number CMMI 1663363. Any opinions, findings, conclusions or recommendations expressed in this study are those of the authors and do not necessarily reflect the views of the National Science Foundation.

References

Church, C.R., Snow, J.T., Baker, G.L., Agee, E.M., 1979. Characteristics of tornado-like vortices as a function of swirl ratio: a laboratory investigation. J. Atmos. Sci. 36, 1755–1776.

Davies-Jones, R.P., 1973. The dependence of core radius on swirl ratio in a tornado simulator. J. Atmos. Sci. 30, 1427–1430.

Eguchi, Y., Hattori, Y., Nakao, K., James, D., Zuo, D., 2018. Numerical pressure retrieval from velocity measurement of a turbulent tornado-like vortex. J. Wind Eng. Ind. Aerod. 174, 61–68.

Feng, C., Chen, X., 2018. Characterization of translating tornado-induced pressures and responses of a low-rise building frame based on measurement data. Eng. Struct. 174, 495–508.

Haan Jr., F.L., Balaramudu, V., Sarkar, P.P., 2010. Tornado-Induced wind loads on a low-rise building. J. Struct. Eng. 136, 106–116.

Haan Jr., F.L., Sarkar, P.P., Gallus, W.A., 2008. Design, construction and performance of a large tornado simulator for wind engineering applications. Eng. Struct. 30, 1146–1159.

Karami, M., Hangan, H., Carassale, L., Peerhossaini, H., 2019. Coherent structures in tornado-like vortices. Phys. Fluids 31, 085118.

Letchford, C., Levitz, B., James, D., 2015. Internal Pressure Dynamics in Simulated Tornadoes. Structures Congress 2015. American Society of Civil Engineers, pp. 2689–2701.

Lewellen, D.C., Lewellen, W.S., Xia, J., 2000. The influence of a local swirl ratio on tornado intensification near the surface. J. Atmos. Sci. 57, 527–544.

Lewellen, W.S., 1962. A solution for three-dimensional vortex flows with strong circulation. J. Fluid Mech. 14, 420–432.

Pauley, R.L., Church, C.R., Snow, J.T., 1982. Measurements of maximum surface pressure deficits in modeled atmospheric vortices. J. Atmos. Sci. 39, 369–377.

Rajasekharan, S.G., Matsui, M., Tamura, Y., 2013. Characteristics of internal pressures and net local roof wind forces on a building exposed to a tornado-like vortex. J. Wind Eng. Ind. Aerod. 112, 52–57.

Razavi, A., Sarkar, P.P., 2018. Tornado-induced wind loads on a low-rise building: influence of swirl ratio, translation speed and building parameters. Eng. Struct. 167, 1–12.

Refan, M., Hangan, H., 2016. Characterization of tornado-like flow fields in a new model scale wind testing chamber. J. Wind Eng. Ind. Aerod. 151, 107–121.

Refan, M., Hangan, H., Siddiqui, K., 2015. Physical Modelling of Tornado-like Flow Field. ASME-JSME-KSME 2015 Joint Fluids Engineering Conference, Seoul, Korea.

Roueche, D.B., Prevatt, D.O., Haan, F.L., 2020. Tornado-Induced and straight-line wind loads on a low-rise building with consideration of internal pressure. Frontiers in Built Environment 6.

Sabareesh, G.R., Matsui, M., Tamura, Y., 2012. Dependence of surface pressures on a cubic building in tornado like flow on building location and ground roughness. J. Wind Eng. Ind. Aerod. 103, 50–59.

Snow, J.T., Church, C.R., Barnhart, B.J., 1980. An investigation of the surface pressure fields beneath simulated tornado cyclones. J. Atmos. Sci. 37, 1013–1026.

Tang, Z., Feng, C., Wu, L., Zuo, D., James, D.L., 2018a. Characteristics of tornado-like vortices simulated in a large-scale ward-type simulator. Boundary-Layer Meteorol. 166, 327–350.

Tang, Z., Zuo, D., James, D., Eguchi, Y., Hattori, Y., 2018b. Effects of aspect ratio on laboratory simulation of tornado-like vortices. Wind Struct. 27, 111–121.

Tari, A.P., Gurka, R., Hangan, H., 2010. Experimental investigation of tornado-like vortex dynamics with swirl ratio: the mean and turbulent flow fields. J. Wind Eng. Ind. Aerod. 98, 936–944.

Thampi, H., Dayal, V., Sarkar, P.P., 2011. Finite element analysis of interaction of tornados with a low-rise timber building. J. Wind Eng. Ind. Aerod. 99, 369–377.

Wang, J., Cao, S., Pang, W., Cao, J., 2017. Experimental study on effects of ground roughness on flow characteristics of tornado-like vortices. Boundary-Layer Meteorol. 162, 319–339.

Ward, N.B., 1972. The exploration of certain features of tornado dynamics using a laboratory model. J. Atmos. Sci. 29, 1194–1204.

Ying, S.J., Chang, C.C., 1970. Exploratory model study of tornado-like vortex dynamics. J. Atmos. Sci. 27, 3–14.